Weber & Maas (Eds.)
Progress in Brain Research, Vol. 161
ISSN 0079-6123

CHAPTER 26

In vivo tracking of stem cells in brain and spinal cord injury

Eva Sykova* and Pavla Jendelova

Institute of Experimental Medicine ASCR, EU Centre of Excellence, Prague, Czech Republic; Center for Cell Therapy and Tissue Repair, Charles University, Second Medical Faculty, Prague, Czech Republic; Department of Neuroscience, Charles University, Second Medical Faculty, Prague, Czech Republic

Abstract: Cellular magnetic resonance (MR) imaging is a rapidly growing field that aims to visualize and track cells in living organisms. Superparamagnetic iron oxide (SPIO) nanoparticles offer a sufficient signal for T2 weighted MR images. We followed the fate of embryonic stem cells (ESCs) and bone marrow mesenchymal stem cells (MSCs) labeled with iron oxide nanoparticles (Endorem®) and human $CD34^+$ cells labeled with magnetic MicroBeads (Miltenyi) in rats with a cortical or spinal cord lesion, models of stroke and spinal cord injury (SCI), respectively. Cells were either grafted intracerebrally, contralaterally to a cortical photochemical lesion, or injected intravenously. During the first post-transplantation week, grafted MSCs or ESCs migrated to the lesion site in the cortex as well as in the spinal cord and were visible in the lesion on MR images as a hypointensive signal, persisting for more than 30 days. In rats with an SCI, we found an increase in functional recovery after the implantation of MSCs or a freshly prepared mononuclear fraction of bone marrow cells (BMCs) or after an injection of granulocyte colony stimulating factor (G-CSF). Morphometric measurements in the center of the lesions showed an increase in white matter volume in cell-treated animals. Prussian blue staining confirmed a large number of iron-positive cells, and the lesions were considerably smaller than in control animals. Additionally, we implanted hydrogels based on poly-hydroxypropylmethacrylamide (HPMA) seeded with nanoparticle-labeled MSCs into hemisected rat spinal cords. Hydrogels seeded with MSCs were visible on MR images as hypointense areas, and subsequent Prussian blue histological staining confirmed positively stained cells within the hydrogels. To obtain better results with cell labeling, new polycation-bound iron oxide superparamagnetic nanoparticles (PC-SPIO) were developed. In comparison with Endorem, PC-SPIO demonstrated a more efficient intracellular uptake into MSCs, with no decrease in cell viability. Our studies demonstrate that magnetic resonance imaging (MRI) of grafted adult as well as ESCs labeled with iron oxide nanoparticles is a useful method for evaluating cellular migration toward a lesion site.

Keywords: cell transplantation; iron oxide nanoparticles; magnetic resonance; MicroBeads; photochemical lesion; scaffold; spinal cord injury

Introduction

Stem cells and progenitor cells are being explored in regenerative medicine for cell therapy in disorders of the central nervous system (CNS; Park et al., 2002; McKay, 2004; Newman et al., 2004; Roitberg, 2004; Emsley et al., 2005; Fairless and Barnett, 2005; Pluchino et al., 2005; Zhao et al., 2005; Uccelli et al., 2006). Crucial to the future success of cell transplantation in the clinical setting is the ability of transplanted cells to migrate

*Corresponding author. Tel.: +420-241062230; Fax: +420-241062782; E-mail: sykova@biomed.cas.cz

DOI: 10.1016/S0079-6123(06)61026-1

from the site of transplantation to the lesioned area and to survive, differentiate, and/or produce growth factors and cytokines for the prolonged periods of time necessary for the patient to benefit from their regenerative properties. Visualizing transplanted cells in vivo is essential for preclinical studies in rodents, and the magnetic tracking of cells appears to be a valuable tool for such studies. Magnetic resonance (MR) imaging may also serve to study cell migration to lesions, its timecourse, and how long the cells persist in the target region. Such information could help to elucidate the time window during which the transplantation of therapeutic cells may be clinically effective, the number of cells needed, and the optimal method of their administration. For magnetic resonance imaging (MRI) detection, cells can be labeled with MR contrast agents in order to make them visible in vivo (Bulte et al., 2002; Jendelova et al., 2003, 2004; Sykova and Jendelova, 2005, 2006; Sykova et al., 2006).

Superparamagnetic cell labels

Superparamagnetic iron oxide (SPIO) nanoparticles were introduced as contrast agents shortly after the use of gadolinium-chelates (Mendonca Dias and Lauterbur, 1986; Renshaw et al., 1986; Pachernik et al., 2005). They are currently preferred as contrast agents primarily due to the following properties: (a) they provide the greatest signal contrast change, in particular on T2 and T2* weighted images; (b) they are composed of biodegradable iron; (c) their surface coating makes them soluble and stable and allows for the chemical linkage of functional groups and ligands; and (d) they can be easily detected by both light and electron microscopy (EM; Jendelova et al., 2003; Bulte and Kraitchman, 2004).

Iron oxide nanoparticle stabilization in order to prevent aggregation is most commonly accomplished by a surface coating of dextran. Dextran-coated SPIO nanoparticles include the products Feridex® and Endorem®, the ultrasmall superparamagnetic iron oxide (USPIO) nanoparticles Combidex® and Sinerem®, monocrystalline iron oxide nanoparticles, and cross-linked iron oxide nanoparticles. Another approach for stabilizing iron oxide nanoparticles is the use of carboxylated polyamidoamine dendrimers (Bulte et al., 2001). These highly soluble nanocomposites of iron oxides and dendrimers are stable under a wide range of temperatures and pH and have an overall size of 20–30 nm.

Iron oxide nanoparticles also require an appropriate outer surface layer that induces the internalization of the particles into the cytoplasm, so that they can be nonspecifically taken up by a variety of cultured mammalian cells, regardless of cell origin or animal species. In magnetodendrimers, the highly charged carboxylated dendrimers bind to multiple sites on the cell membrane, inducing membrane bending followed by endocytosis (Zhang and Smith, 2000). In the case of anionic magnetic nanoparticles, the negative surface charge induces an uptake three orders of magnitude greater than that of conventional dextran-coated SPIO nanoparticles (Billotey et al., 2003). A disadvantage of these particles, as well as of the magnetodendrimers, is that they have not yet been commercially developed. Another method is based on the mixing of a commercially available (U)SPIO formulation, Feridex® (Frank et al., 2003) or Sinerem®, and a commercially available transfection agent, for example poly-L-lysine, Lipofectamin, or Fugene™ (Frank et al., 2003). We have developed new polycation-bound iron oxide superparamagnetic nanoparticles (PC-SPIO) that can be used for intracellular labeling (Horak et al., 2006).

Cell labeling with dextran-coated SPIO nanoparticles

MR tracking of stem and progenitor cells in the lesioned CNS has been performed by several groups that utilized different methods of administration. The first studies of imaging cell transplants labeled by superparamagnetic contrast agents in rat brains were reported in 1992 (Norman et al., 1992; Hawrylak et al., 1993). Rats received grafts of fetal rat tissue prepared as cell suspensions and

labeled by incubation with reconstituted Sendai viral envelopes containing iron oxide particles. When magnetically labeled neurospheres were transplanted into the ventricles of experimental allergic encephalomyelitis (EAE) rats at the peak of their disease, the migration of glial precursors into white matter structures was observed on MR images (Bulte et al., 2003). Ferromagnetic-labeled neural progenitor cells were also transplanted into the cisterna magna of rats that underwent experimental MCAO (middle cerebral artery occlusion). MR images showed the migration of cells throughout the ventricular system toward the ischemic brain parenchyma (Zhang et al., 2003). Olfactory ensheathing cells (OECs) labeled with magnetodendrimers were implanted into the transected rat spinal cord, and their distribution was followed in vivo using MR imaging (Lee et al., 2004). In our experiments (Jendelova et al., 2003, 2004), we have shown that a suitable contrast agent for mesenchymal stem cells (MSCs), embryonic stem cells (ESCs), and OECs is a commercially available contrast agent based on dextran-coated SPIO nanoparticles (Fig. 1A), Endorem® (Guerbet, France), which has also been approved as a blood pool agent for human use. The contrast agent Endorem can be easily incorporated by endocytosis, and all the cells survive and further divide in vitro. Therefore, Endorem uptake does not need to be facilitated by a transfection agent, which can damage large numbers of cells (Arbab et al., 2004).

Bone marrow-derived MSCs are adult stem cells that reside within the bone marrow compartment. Recent data have presented evidence for their multilineage differentiation potential (Pittenger et al., 1999). More recently, MSCs have been reported to have the ability to stimulate or participate in the regeneration of diverse tissues and organs, including the liver, myocardium, endothelium, and CNS (Takahashi et al., 1999; Orlic et al., 2001a, b; Jiang et al., 2002; Toma et al., 2002). In addition, they can be genetically modified, and, due to their migratory properties, they can serve as a carrier for drug delivery in tumor therapies (Anderson et al., 2005). In cell therapy, bone marrow cells (BMCs) have some advantages over other sources of cells: (a) they are relatively easy to isolate; (b) they can be used in autologous transplantation protocols; and (c) they have already been approved for the treatment of hematopoietic diseases.

In our experiments, cell cultures of human MSCs or rat MSCs were incubated 2–3 days in media containing Endorem. Nanoparticles were detected by staining for iron (Fig. 1B). Transmission electron microscopy confirmed the presence of iron oxide particles inside the cells, observed as large membrane-bound clusters scattered within the cell cytoplasm (Fig. 1C). On the day that nanoparticles were withdrawn, the efficiency of MSC labeling (i.e., how many cells of the total number of analyzed cells were labeled) was 50–70%.

Tracking mesenchymal stem cells in an experimental model of stroke

Endorem-labeled MSCs were co-labeled with bromdeoxyuridine (BrdU) and grafted into rats with a cortical photochemical lesion (Jendelova et al., 2003). Rats were examined weekly for a period of 3–7 weeks post-transplantation using a 4.7 T Bruker spectrometer. Single sagittal, coronal, and transversal images were obtained by a fast gradient echo sequence for localizing subsequent T2 weighted transversal images measured by a standard turbospin echo sequence. The lesion was clearly visible on MR images 2 h after lesioning as a hyperintense signal and remained visible during the entire measurement period. No recognizable hypointense signal in the lesion was detected during the first 2 days after implantation. A decrease in the MR signal was found only at the injection site in animals with cells injected contralaterally to the lesion. One week after grafting, we observed a hypointense signal in the lesion, which intensified during the second and third weeks (Fig. 1D). Histology confirmed that a large number of Prussian blue-positive cells had entered the lesion. No hypointense signal was found in other brain regions. The hypointense signal occurred only in damaged areas populated with MSCs, and its intensity corresponded to Prussian

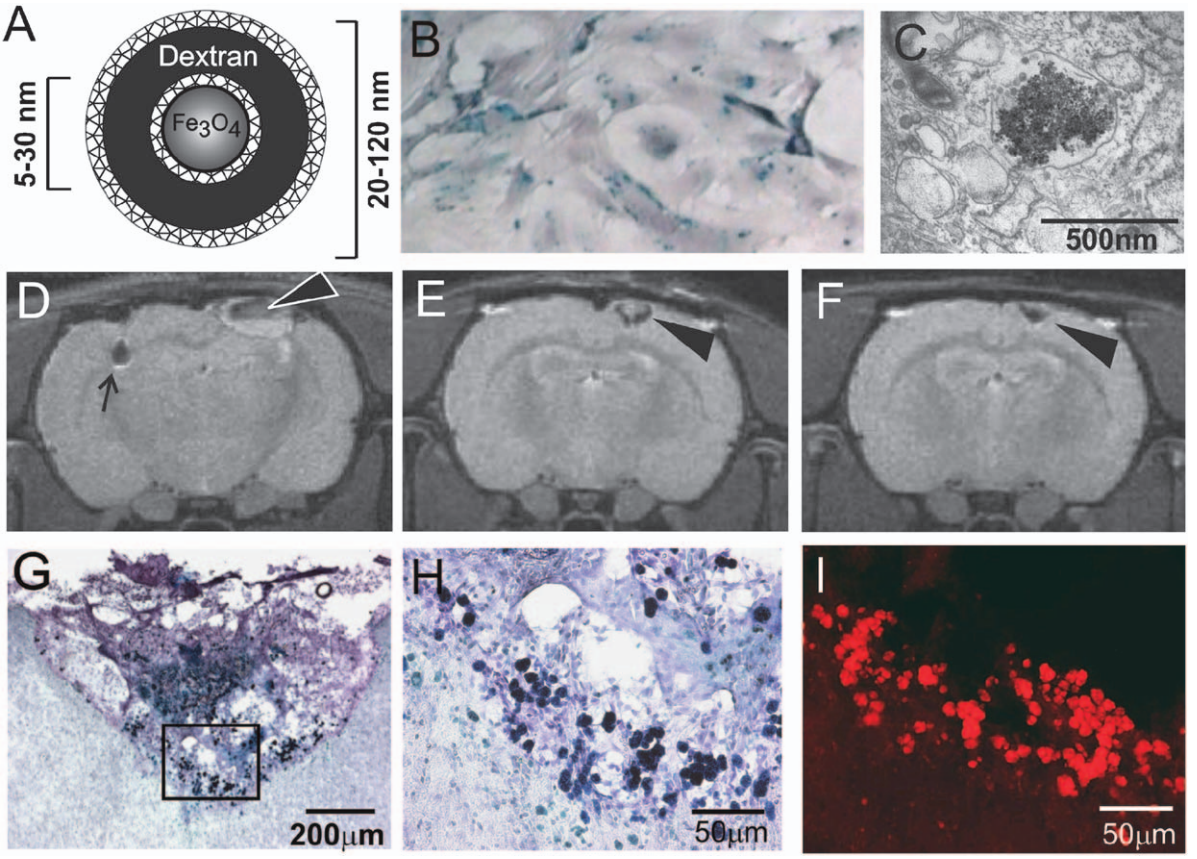

Fig. 1. (A) Scheme of an iron oxide nanoparticle. The contrast agent Endorem consists of a superparamagnetic Fe_3O_4 core coated by a dextran shell. (B) Rat mesenchymal stem cells (MSCs) in culture labeled with superparamagnetic nanoparticles (blue dots). The cell nuclei are counterstained with hematoxylin. (C) Transmission electron microphotograph of a cluster of iron nanoparticles surrounded by a cell membrane. (D) An implant of Endorem-BrdU co-labeled MSCs (in the hemisphere contralateral to the lesion, arrow) and the lesion (arrowhead) itself are both hypointense in an MR image taken 2 weeks after implantation. (E), (F) A hypointense signal (black arrowhead) was observed in the lesion 6 days after the intravenous (i.v.) injection of Endorem-BrdU co-labeled MSCs, becoming more hypointense and persisting for 47 days (F). (G, H) Massive invasion of rat MSCs (Prussian blue staining counterstained with hematoxylin) into a photochemical lesion 7 weeks after i.v. injection into a rat with a photochemical lesion. (I) Serial section stained for BrdU, 7 weeks after i.v. injection. (Adapted with permission from Jendelova et al. (2003).)

blue or BrdU staining. Only a few (less than 3%) of the MSCs that migrated into the lesion expressed the neuronal marker NeuN when tested 28 days post-implantation. No GFAP-positive cells were found in the lesion.

After the intravenous injection of MSCs, we found a similar hypointense MR signal in the lesion site. The signal was observed 6 days after cell infusion and persisted for 7 weeks (Figs. 1E, F). Prussian blue and anti-BrdU staining confirmed the presence of iron oxide-BrdU co-labeled cells in the lesion, which densely populated the borders of the lesion (Figs. 1G–I).

Only a few cells weakly stained for Prussian blue were found in photochemical lesions without any implanted cells. The staining represents iron, which most likely originated in hemorrhages and iron degradation products released from iron-containingproteins (such as hemoglobin, ferritin, and hemosiderin) and phagocytized by microglia/macrophages. We did not observe any BrdU-positive cells in the brains of nongrafted animals.

Tracking embryonic stem cells in an experimental model of stroke

ESCs are pluripotent cell lines with a capacity for self-renewal and broad differentiation plasticity. They are derived from embryos and can be propagated as a homogeneous, uncommitted cell population for an almost unlimited period of time without losing their pluripotency and their stable karyotype. Mouse ES cell-derived glial precursors, transplanted into rats with myelin disease, interacted with the host neurons to produce myelin in the brain and spinal cord (Brustle et al., 1999). Retinoic acid-treated embryoid bodies from mouse ESCs, when transplanted into rat spinal cord 9 days after traumatic injury, differentiated into astrocytes, oligodendrocytes, and neurons and promoted recovery (McDonald et al., 1999). Bjorklund et al. (2002) reported that undifferentiated mouse ESCs can become dopamine-producing neurons in the brain in a rat model of Parkinson's disease and can lead to partial functional recovery.

We used mouse ESCs transfected with the pEGFP-C1 vector (Pachernik et al., 2005) and labeled with SPIO nanoparticles (Jendelova et al., 2004). Since undifferentiated ESCs may form embryonic tumors when grafted into a host animal, we induced neural differentiation by culturing enhanced green fluorescent protein (eGFP) ESCs in serum containing DMEM (Dulbecco's modified Eagle medium)/F12 without leukemia inhibitory factor (LIF) for 2 days and then transferred the cells into serum-free media supplemented with insulin, transferrin, selenium, and fibronectin for further culture (Pachernik et al., 2005). Feeder-free eGFP ESCs were labeled with Endorem (112.4 μg/ml) during three passages (Fig. 2A). Cell counting of Prussian blue stained cells in suspension revealed that the labeling efficiency was ~80%. Cells were transplanted intracerebrally or intravenously on the 8th day of differentiation into adult Wistar rats with a cortical photochemical lesion 1 week after lesioning (Jendelova et al., 2004), and were detected by staining for iron and by GFP fluorescence. When we implanted the ESCs 7 days post-lesion, we found a massive migration of Endorem-labeled GFP-positive cells into the lesion site regardless of the route of administration (Fig. 2D). We observed very similar MR images to those obtained after the implantation of MSCs. In rats with a photochemical lesion and contralaterally injected cells, the cell implants were visible as a hypointense area at the injection site. Two weeks after grafting, a hypointense signal was also observed in the corpus callosum and in the lesion (Fig. 2B). At the same time, histology showed that a large number of Prussian blue-positive cells had entered the lesion. Many labeled cells were also detected in the corpus callosum, suggesting a migration from the contralateral hemisphere toward the lesion (Fig. 2C). When the ESCs were injected intravenously into lesioned rats, we found a hypointense MR signal only at the site of the lesion. However, the extent of the differentiation of eGFP ESCs labeled with nanoparticles, and found in the lesion, was much greater than with grafted MSCs. Of all the eGFP ESCs containing nanoparticles found in the lesion, 70% of them proved to be astrocytes, very few (less than 1%) were oligodendrocytes, and ~5% of nanoparticle-labeled eGFP ESCs had differentiated into neurons (Jendelova et al., 2004). Electron microscopy revealed mature astrocytes, neurons, and oligodendrocytes in the lesion site containing iron oxide nanoparticles, providing strong supporting evidence that these cells differentiated in the lesion from implanted embryonic cells (Figs. 2E, F).

Tracking mesenchymal stem cells in a rat model of spinal cord injury

Evaluating the effect of different BMC populations on morphological and functional recovery after spinal cord injury (SCI) is an important aspect of our preclinical research. In rats with a balloon-induced spinal cord compression lesion, we studied the effect of an intravenous injection of Endorem-labeled nonhematopoietic MSCs (Urdzikova et al., 2006). The results obtained were compared with those following the implantation of a freshly isolated mononuclear fraction of bone marrow containing stromal cells, hematopoietic and nonhematopoietic stem and precursor cells, and lymphocytes (BMCs). Furthermore, we studied the effect of granulocyte colony stimulating factor (G-CSF) mobilization of endogenous BMCs containing mainly

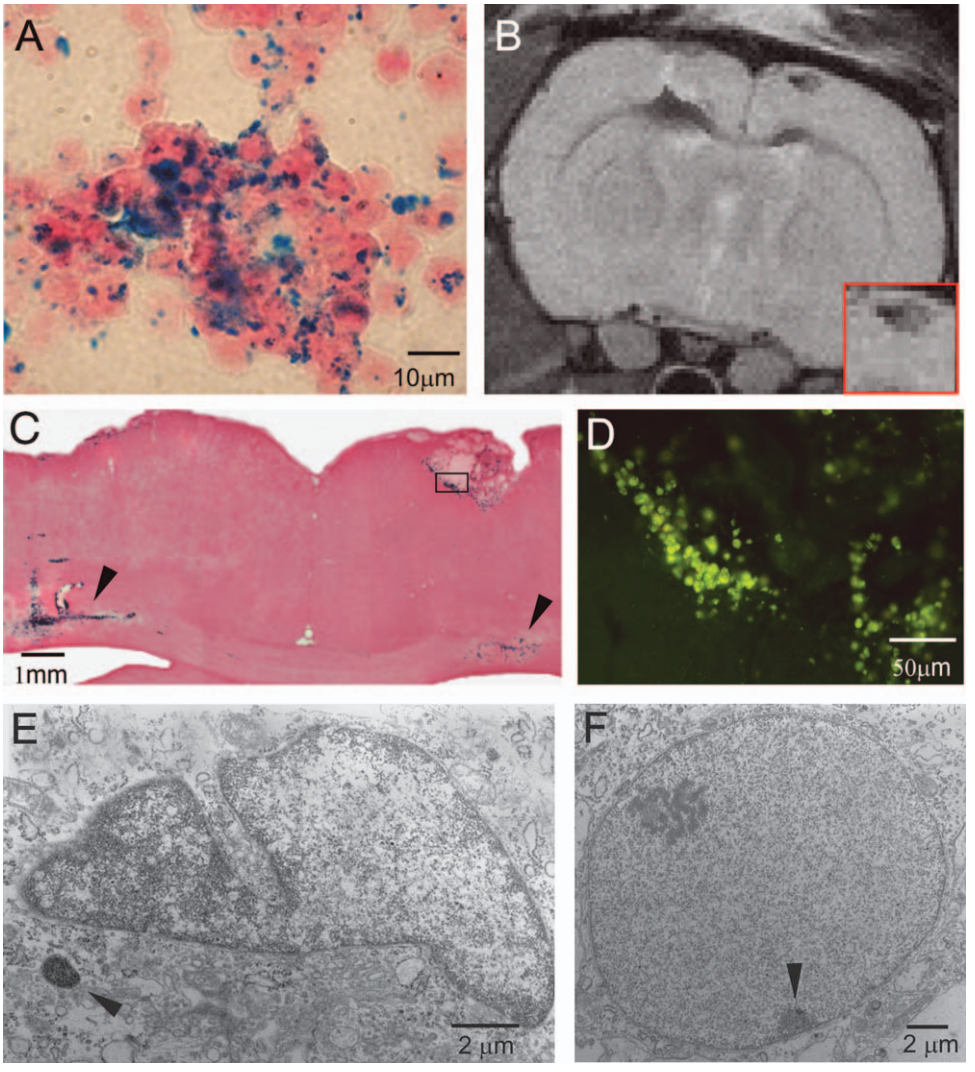

Fig. 2. (A) Trypsinized nanoparticle-labeled suspensions of ESCs after the third passage. (B) The cell implant (in the hemisphere contralateral to the lesion) and the lesion are hypointense in MR images 2 weeks after implantation. A hypointensive signal is also found in the corpus callosum. (C) Dense Prussian blue staining of the injection site in the contralateral hemisphere, the corpus callosum, and the photochemical lesion, 4 weeks after grafting. (D) Invasion of GFP-labeled cells showing GFP-positive ESCs in the lesion 4 weeks after the i.v. injection of eGFP ESCs (serial section to the slice shown in Fig. 2C). (E) Astrocyte from the brain tissue of a rat with nanoparticle-labeled eGFP ESCs implanted contralaterally to the lesion; the nanoparticles are visible in small dense clusters in the cell cytoplasm (arrowhead). (F) Neuron with nanoparticles marginated to the nuclear membrane. (Adapted with permission from Jendelova et al. (2004).)

hematopoietic stem cells, along with progenitor cells and lymphocytes (Sasaki et al., 2001; Akiyama et al., 2002).

MSCs labeled with Endorem were injected intravenously into the femoral vein 1 week after lesioning. MR images were taken ex vivo 4 weeks after implantation using a standard whole body resonator. Functional status was assessed weekly for 5 weeks after spinal cord lesioning, using the Basso-Beattie-Bresnehan (BBB) locomotor rating score and the plantar test. Our data indicated that lesioned animals with grafted MSCs had higher

locomotor scores as indicated by their BBB scores and showed better responses in sensitivity testing using the plantar test than did control animals. Particularly, the plantar test showed the recovery of sensitivity in the hind limbs. On MR images we observed the lesion as an inhomogeneity in the tissue texture with a hyperintense signal only in the area of the SCI (Fig. 3A). Images of longitudinal spinal cord sections from animals grafted with nanoparticle-labeled MSCs showed the lesion as a dark hypointense area (Fig. 3B). Prussian blue staining confirmed a large number of positive cells present in the lesion site (Fig. 3C). On serial sections, Prussian blue-positive cells corresponded to cells labeled with PKH 26, as seen in (Figs. 3D, E). To exclude the possibility that free nanoparticles were taken up by macrophages, we performed immunohistochemical and Prussian blue staining to co-localize iron in activated microglia/macrophages. Although we found strong positive staining for macrophages in the lesions using ED1 antibody, Prussian blue staining did not,

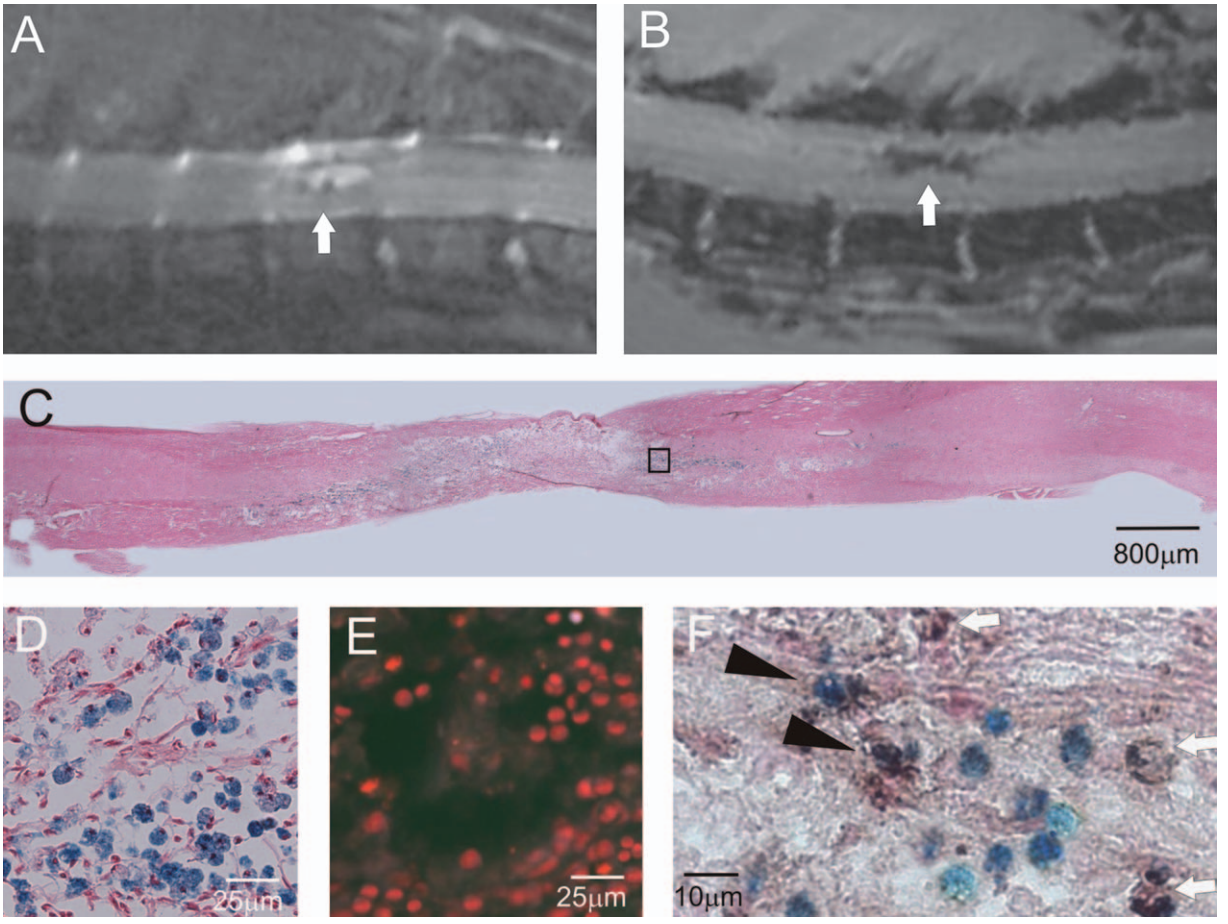

Fig. 3. (A) Longitudinal MR image of a spinal cord lesion 5 weeks after induction. The formation of the lesion cavity is visible as a strong hyperintensive signal (arrow). (B) Longitudinal MR image 4 weeks after MSC grafting. The lesion with nanoparticle-labeled cells is visible as a dark hypointensive area (arrow). (C) Prussian blue staining of a lesion populated with nanoparticle-labeled MSCs (blue dots). (D) Magnified region from Fig. C. (E) Intravenously injected MSCs were also detectable in the spinal cord lesion using the membrane florescent dye PKH 26. Serial section to D. (F) Immunostaining with ED-1 antibody revealed a number of macrophages in the lesion (white arrows). The majority of Prussian blue-positive cells did not co-localize with ED-1 staining; however, a few macrophages were Prussian blue-positive (black arrowheads). (Adapted with permission from Urdzikova et al. (2006).)

for the most part, co-localize with the ED1 staining (Fig. 3F).

Morphometric measurements of the spared white and gray matter were performed in the center of the lesions. The spared cross-sectional area of the white matter, as well as the volume of spared white matter, was significantly greater in MSC-treated animals. The spared cross-sectional area of the gray matter was also significantly larger in MSC-treated animals. In further studies, lesioned animals grafted with BMCs or injected with G-SCF also had higher scores in BBB testing than did control animals and also showed a faster recovery of sensitivity in their hind limbs using the plantar test. However, the functional improvement was more pronounced in MSC-treated rats (Figs. 4A, B). Morphological measurements of the spared cross-sectional area of the white matter showed a statistically significant increase in groups treated with BMCs or G-SCF, compared to controls, cranially to the lesion center; a statistically significant increase in the volume of spared white

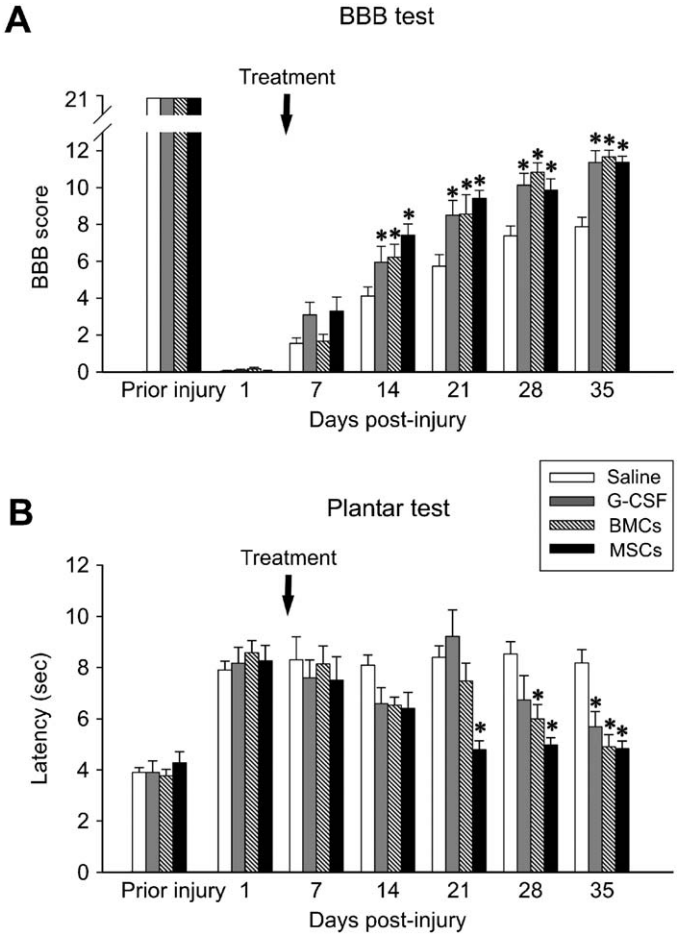

Fig. 4. (A) Behavioral open field BBB motor scores of MSC, BMC, and G-CSF treated rats were significantly higher than those of saline-injected (control) animals, 14, 21, 28, and 35 days after SCI ($p < 0.05$). The scores of the MSC, BMC, and G-CSF treated animals were not significantly different from one another at any time point. (B) Time course of the animals' response to radiant heat measured with the plantar test in treated and saline-injected rats. In all treated rats, the latency times decreased as their recovery progressed. The most pronounced effect was seen in MSC treated rats. The latency time in the saline-injected (control) rats did not change during the 35 days survival period. Data are averaged between right and left hind limbs and expressed as mean $\pm$ SEM. *$p < 0.05$ compared to control group. (Adapted with permission from Urdzikova et al. (2006).)

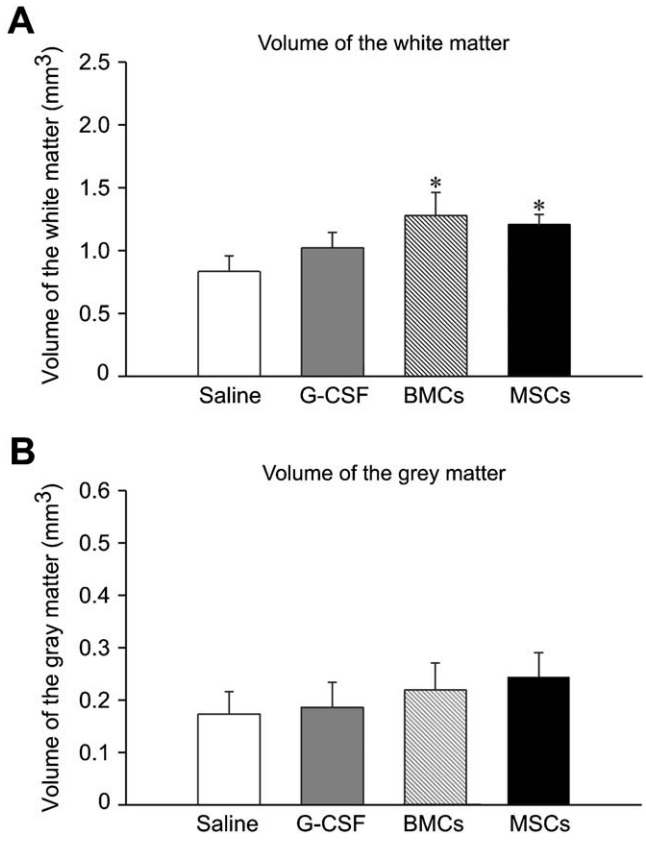

Fig. 5. (A) The total volume of the white matter in 11 mm long segments of the spinal lesion in MSCs, BMCs, and G-CSF-treated and saline-injected animals. (B) The total volume of gray matter in 11 mm long segments of the spinal lesion in MSCs, BMCs, and G-CSF-treated and saline-injected animals. No statistically significant differences were observed between treated and saline-injected animals. All data are presented as means ± SEM. *$p < 0.05$ compared to saline-injected (control) rats. (Adapted with permission from Urdzikova et al. (2006).)

matter was observed in the BMC-treated group. The spared white matter volume in the G-CSF-treated rats was also increased, but the increase did not reach statistical significance (Fig. 5).

Stem cell labeling with polycation-bound nanoparticles

In all the above-described experiments, dextran-coated SPIO nanoparticles (the contrast agent Endorem) were used as an intracellular label. However, the efficiency of the cell labeling was maximally 70%. In addition, on the day of particle withdrawal a decrease in cell viability (using the WST1 colorimetric assay) was observed. We therefore developed new polycation-bound SPIO nanoparticles (Fig. 6A; Horak et al., 2006). We compared the influence of both types of nanoparticles on cell viability and labeling efficiency in rat and human MSCs. The PC-SPIO nanoparticle suspension was used at a much lower iron concentration per milliliter of culture media (15.4 μg/ml), and the cells were incubated with PC-SPIO for 3 days. The results were compared with Endorem labeling (Tables 1 and 2). The measurements were performed on the day of withdrawal of the nanoparticles (day 3) and 4 days later (day 7).

Labeling cells with PC-SPIO nanoparticles was more efficient than labeling with Endorem, i.e., more cells from the total number of analyzed cells were labeled with PC-SPIO nanoparticles than

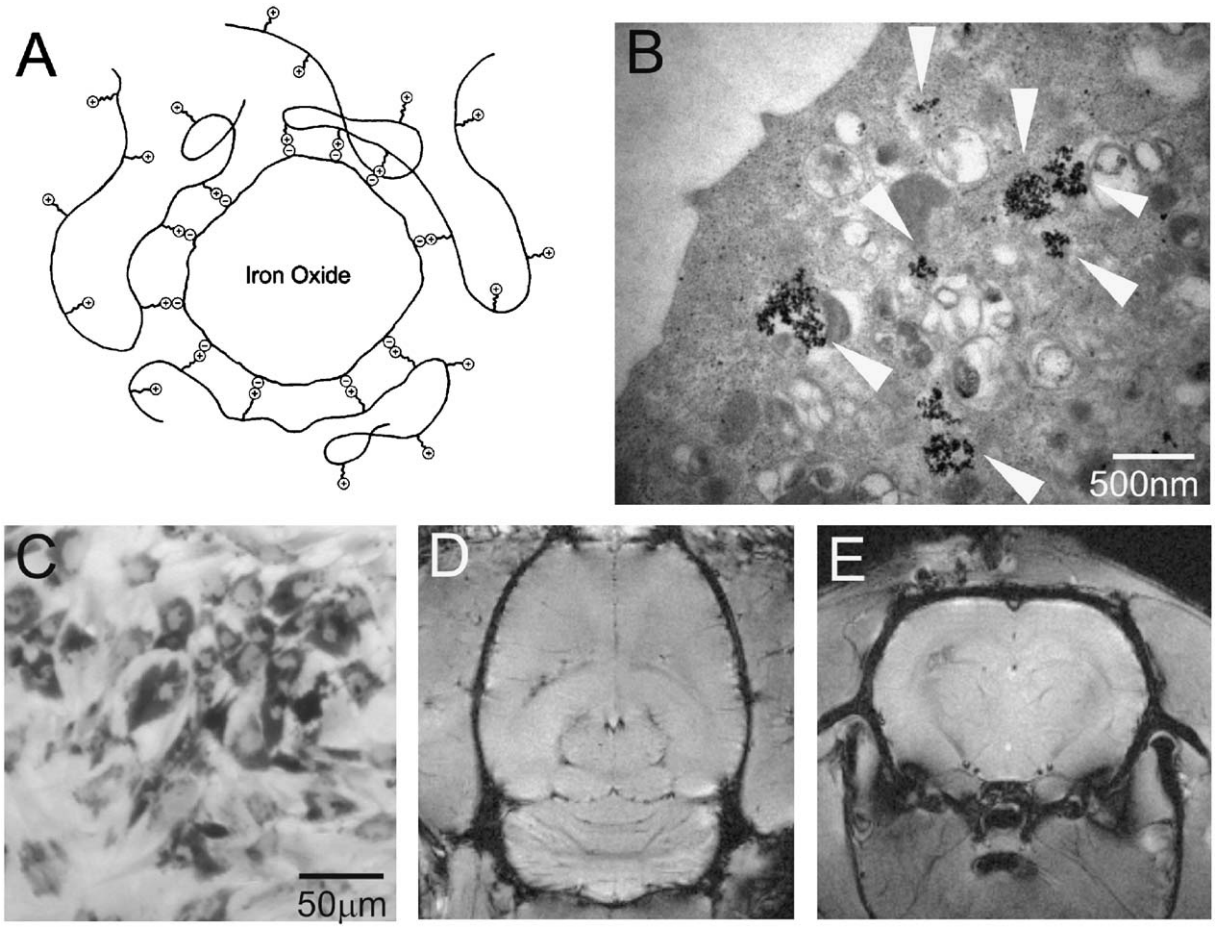

Fig. 6. (A) Schematic illustration of a polycation-bound superparamagnetic iron oxide nanoparticle. (B) Transmission electron photomicrograph of MSCs labeled with PC-SPIO showing clusters of iron nanoparticles (arrows) in the cell cytoplasm, which are not surrounded by a cell membrane. (C) Prussian blue staining of MSCs in culture labeled with PC-SPIO. (D, E) Axial and coronal (E) MR images of a rat brain with 1000 cells labeled with PC-SPIO implanted to the left hemisphere and 1000 Endorem-labeled cells implanted to the right hemisphere. MR images were taken 3 days after implantation.

Table 1. The percentage of cells labeled with nanoparticles after 3 days incubation

	Endorem-labeled cells (%)	PC-SPIO-labeled cells (%)
Rat MSCs	59.3	92.2
Human MSCs	65.2	87.5

with Endorem (Table 1; Fig. 6C). In Table 2 the cell viability of labeled cells is expressed as a percentage of the number of viable unlabeled cells (taken as the control value and defined as 100%). In Endorem-labeled human MSCs, on day 3 the cell viability dropped to 50%; however, within 4 days it recovered to 87%. This transient decrease in cell viability might be due to the relatively high concentration of iron in the culture media (112.4 g/ml), to which some cell cultures might be sensitive. The average amount of iron present in rat MSCs was determined by spectrophotometry after mineralization of iron-labeled cell suspensions. In PC-SPIO-labeled cells, even though the concentration of iron in the culture media was 10 times lower (15.4 μg/ml culture media), the average amount of

Table 2. Cell viability (in %) after incubation with nanoparticles (day 3) and 4 days after withdrawal (day 7)

	Endorem-labeled cells (%)		PC-SPIO-labeled cells (%)	
	Day 3	Day 7	Day 3	Day 7
Rat MSCs	68.9	72.9	92.8	89.7
Human MSCs	49.0	87.0	97.2	98.9

iron was 38 pg/cell, while in Endorem-labeled cells only 17 pg/cell. Transmission electron photomicrographs confirmed that more PC-SPIO nanoparticles were taken up by the rat MSCs than were Endorem nanoparticles (Fig. 6B). Moreover, Endorem was observed as membrane-bound clusters within the cell cytoplasm, indicating an endocytotic process of nanoparticle uptake. The higher cellular uptake of PC-SPIO nanoparticles is possible due to the interaction of the surface coating with the negatively charged cell surface and subsequent endosomolytic uptake. Nanoparticles are transported in endosomes and finally fused with lysosomes, a process during which the vesicle membranes disappear.

To check the sensitivity of the MRI technique and to mimic signal behavior in CNS tissue, suspensions of unlabeled cells and cells labeled with PC-SPIO were imaged in vitro. MR images of 1.7% gelatin phantoms containing iron-labeled MSCs were obtained using a 4.7 T Bruker spectrometer equipped with a standard resonator coil. Even the sample containing the lowest concentration (200 cells/µl, which corresponds on average to 2 cells per image voxel) provided visible contrast compared to a control phantom containing the same number of unlabeled cells. A similar set of experiments was performed in earlier work (Jendelova et al., 2003), in which MR images of gelatin phantoms showed a hypointense signal at concentrations above 625 labeled cells/µl.

For in vivo imaging, rats were examined 3 days post-transplantation in an MR imager. Figure 6 shows that PC-SPIO labeled cells are also clearly recognizable in vivo. The iron oxide-labeled cell implants are visible as a hypointense area at the injection site. Cells labeled by PC-SPIO provide stronger contrast change in the signal than do Endorem-labeled cells (Figs. 6D, E). Labeling with PC-SPIO thus enables the detection of a lower number of cells in the tissue.

Cell labeling with magnetic MicroBeads

The disadvantage of an intracellular label is that it can affect cell metabolism and subsequently cell viability. In addition, these labels are rather nonspecific; they can be loaded by virtually any cell present in the medium. The possibility of labeling only selected cell types would therefore be very useful. In addition, cells labeled and separated by means of immunomagnetic selection would not require in vitro culturing, since the label is attached during separation. This would also allow the immediate clinical use of labeled cells. The first experiments using contrast agents bound to an antibody that can specifically bind to a single cell type were performed by Bulte et al. (1992). They described experiments with human lymphocytes labeled with biotinylated anti-lymphocyte-directed monoclonal antibodies (mabs), to which streptavidin and subsequently biotinylated dextran-magnetite particles were coupled. We tested a new type of specific cell labeling using commercially available cell isolation kits for the magnetic separation of $CD34^+$ cells. $CD34^+$ cells are known as hematopoietic progenitor cells. The cells were separated by means of immunomagnetic selection with anti-CD34 antibodies. For sorting, a SPIO core coated with a polysaccharide that is linked to an antibody is bound to the respective cell (Fig. 7A). The size of the label is comparable to commonly used superparamagnetic MR contrast agents; thus it can provide sufficient contrast on MR images.

Human $CD34^+$ cells from peripheral blood were selected by CliniMACS CD34 Selection Technology (Miltenyi). On EM images, we determined that after cryopreservation, the nanoparticles remained bound to the cell surface, and we observed several iron labels attached to the cell surface (Fig. 7B). Purified $CD34^+$ cells were implanted intracerebrally into rats with a cortical

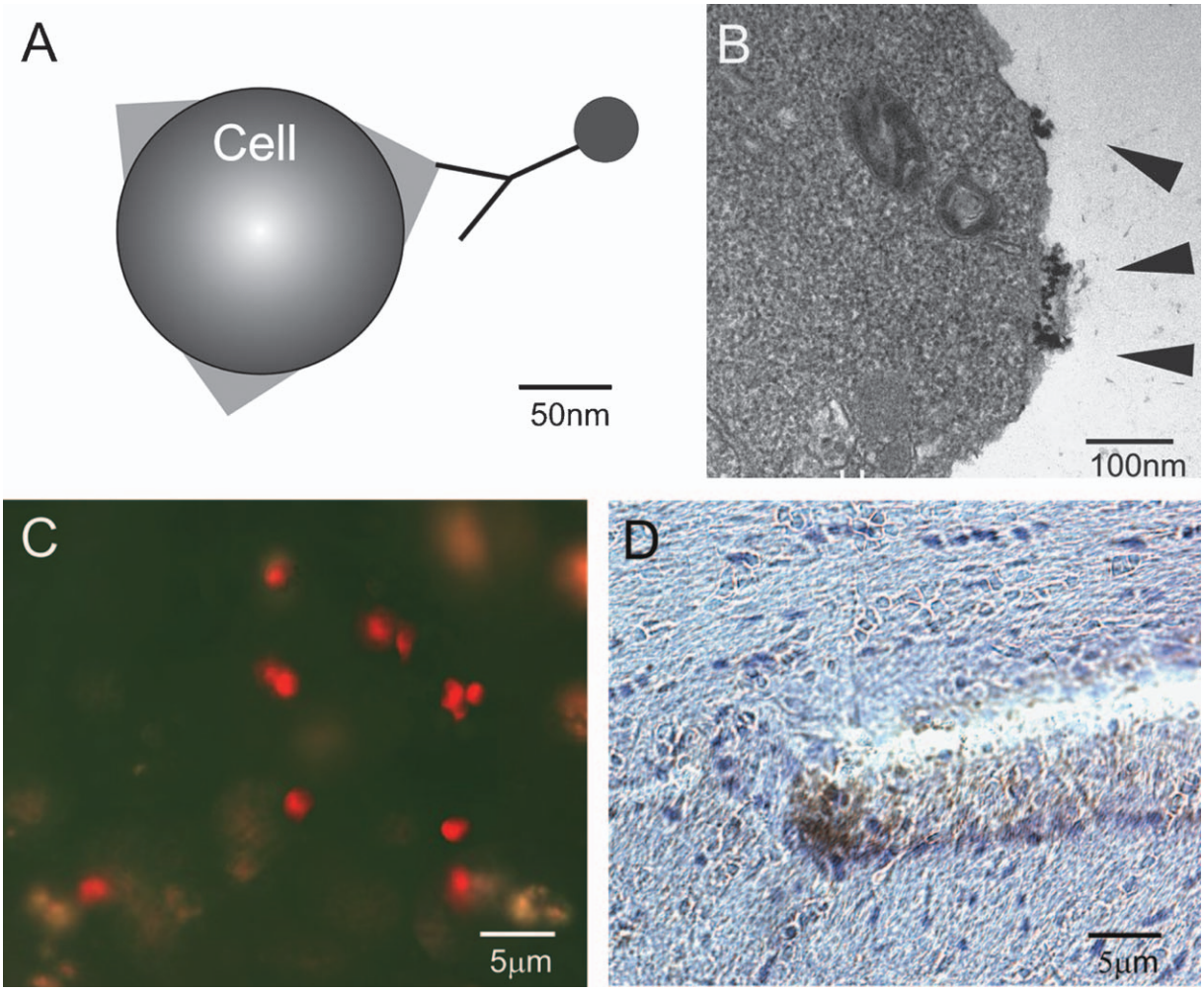

Fig. 7. (A) Scheme of MicroBeads. A superparamagnetic iron oxide core coated with a polysaccharide is linked to an antibody, which in turn is bound to a cell via an antigen–antibody complex. (B) Transmission electron microphotograph of MicroBeads binding to the cell surface. (C) Human cells (positive staining for human nuclei) found in the lesion 4 weeks after the grafting of $CD34^+$ cells. (D) Staining with anti-CD34 revealed $CD34^+$ cells in the subventricular zone. (Adapted with permission from Jendelova et al. (2005).)

photochemical lesion, contralaterally to the lesion (Jendelova et al., 2005; Sykova and Jendelova, 2006). The average iron content per cell, determined by spectrometry, was 0.275 pg. This value is lower by two orders of magnitude than in the case of cell labeling using Endorem or PC-SPIO, which enter the cell (17 or 38 pg, respectively); nevertheless, it still provides sufficient MR contrast (Jendelova et al., 2005).

The cells were detected as a hypointense spot on T2 weighted images 24 h after grafting. The hypointensity of the implant slightly decreased during the first week and then remained without significant changes for the entire measurement period (4 weeks). During the second week, we observed a weak hypointense signal in the lesion that persisted for the next 2 weeks. Prussian blue and anti-human nuclei staining (Fig. 7C) confirmed the presence of magnetically labeled human cells in the corpus callosum and in the lesion. $CD34^+$ cells were detected not only in the corpus callosum and in the lesion, but also in the subventricular

zone (Fig. 7D). Finally, human DNA was detected in the lesioned brain tissue using polymerase chain reaction (PCR), confirming the presence of human cells.

Labeling of stem cells in polymer hydrogels as stem cell carriers

In the case of large lesions, cells alone are not able to repair the injury. It is necessary to bridge the gap left by the lost cell population in order to provide support for tissue restoration, reduce the glial scar, and create a permissive environment for cellular ingrowth and for the diffusion of neuroactive molecules. To bridge such a lesion, we have used biocompatible polymer hydrogels based on poly-hydroxypropylmethacrylamide (HPMA) in combination with stem cell grafting. Before transplantation into a lesion, the hydrogels were seeded in vitro with MSCs. In this case the hydrogels form an inert environment, allowing for the free diffusion of intrinsic growth factors, in which the cells start to differentiate and migrate. The inert and biocompatible environment of the hydrogels also provides an adequate standard background for MR imaging of the cells (Sykova and Jendelova, 2005; Sykova et al., 2006). We employed these cell-polymer constructs in order to facilitate the regeneration of injured spinal cord (Lesny et al., 2006). The right half of a spinal cord segment was removed by hemisection, and a block of HPMA hydrogel seeded with Endorem-labeled MSCs was inserted (Fig. 8A; Sykova and Jendelova, 2005). Six weeks after implantation, the hydrogel had formed a continuous bridge between the hemisected spinal segments, reestablishing the anatomical continuity of the tissue. The hydrogel was visible on MR images as a hypointense area (Fig. 8B), and Prussian blue staining confirmed positively stained cells within the hydrogel (Fig. 8C). Immunostaining for blood vessels (Reca-1, Abcam, UK) confirmed neovascularization of the hydrogel implant (Fig. 8D). Staining for neurofilaments (NF160, Sigma, St. Louis, USA) showed axonal ingrowth into the hydrogel (Fig. 8E; Sykova and Jendelova, 2005; Sykova et al., 2006). Hydrogels seeded with stem cells may therefore serve as an alternative to the conventional grafting of dissociated cells, benefiting from advances in surface chemistry and the cell–cell or cell–matrix interactions that occur during development or regeneration.

Discussion and conclusion

For clinical studies it is obvious that traditional histopathological methods for cell detection are not sufficient to inform us about the migration and fate of the grafted cells in the host tissue. Because of its high spatial resolution, MR imaging is suitable for imaging the distribution of magnetically labeled cells. Labeling methods that use the internalization of iron oxide nanoparticles have some limitations. To label cells with commercially available contrast agents, such as Endorem, a relatively high concentration of iron in the culture media is necessary (Jendelova et al., 2003, 2004). This may cause a transient drop in cell viability, which can be dependent on the type of labeled cell. For improved uptake of magnetic nanoparticles, the surface of the contrast agent needs to be optimized, so that it can induce the internalization of the particles into the cytoplasm. One approach is to use internalizing mabs. The mouse anti-Tfr mab OX-26 induces the internalization of Tft upon binding. Nanoparticles have been conjugated to OX-26 to deliver them to cells by receptor-mediated endocytosis (Bulte et al., 1999). A disadvantage of the use of internalizing mabs, however, is that they are species-specific, and a newly synthesized antibody is required when performing studies in a different animal. In addition, for eventual clinical use, there will be regulatory issues regarding the use of a xenogeneic (i.e., mouse) protein. Recently, a combination of dextran-coated SPIO nanoparticles with a transfection agent has been used (Kalish et al., 2003). When the complexes are added to a cell culture, the transfection agent effectively transports the nanoparticles into the cells through electrostatic interactions. However, each combination of transfection agent and iron oxide nanoparticle has to be carefully titrated and optimized for different cell cultures, since lower concentrations may result in insufficient cellular uptake, whereas higher concentrations may

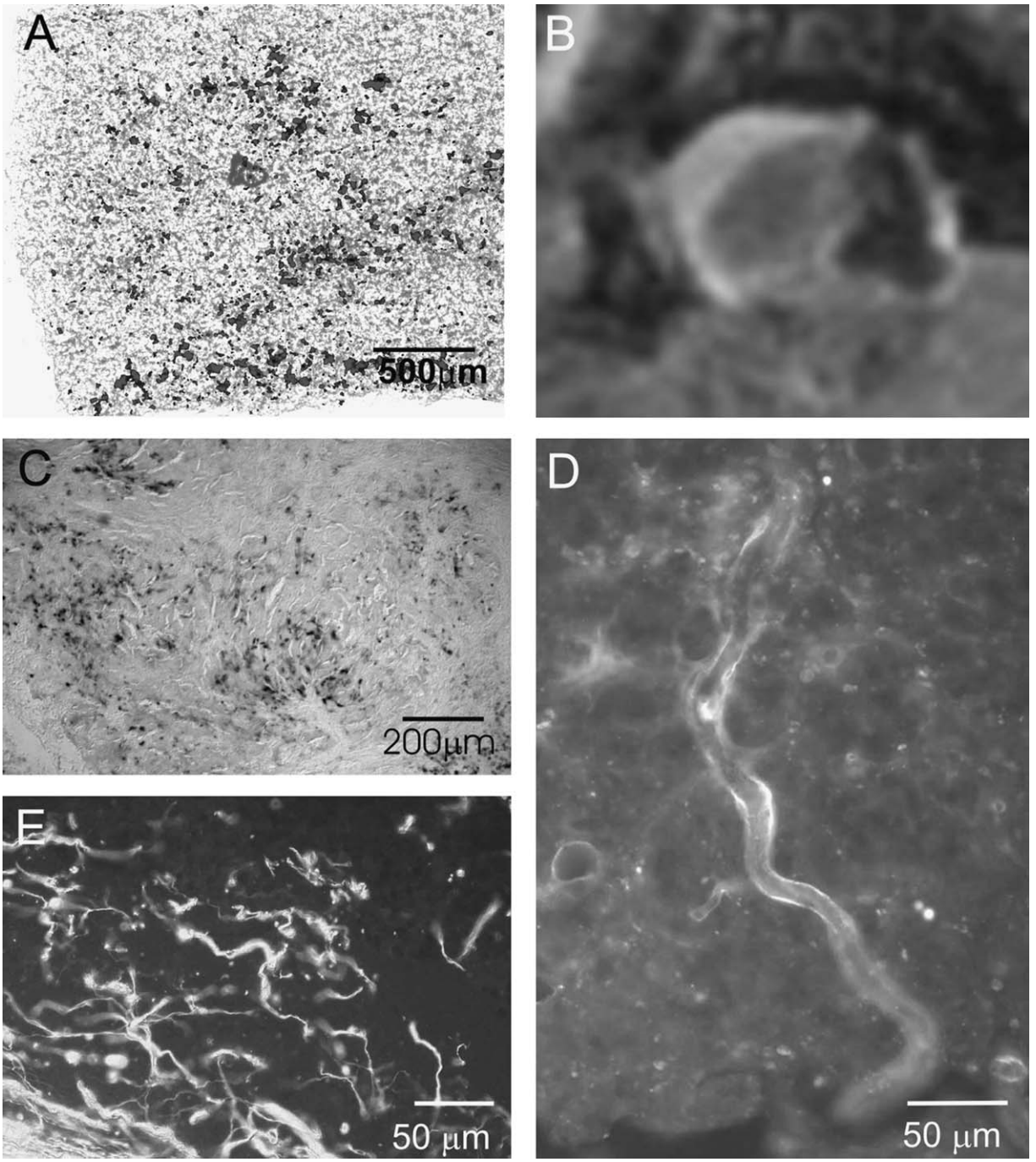

Fig. 8. (A) Endorem-labeled cells seeded into a hydrogel. (B) On MR images 6 weeks after implantation, the hydrogel was visible as a hypointensive area. (C) Prussian blue staining confirmed the presence of Endorem-labeled cells in the hydrogel. (D) Neovascularization of the implant (Reca-1). (E) Ingrowth of NF160-positive axons into the gel.

induce the precipitation of complexes or may be toxic to the cells. In addition, although it has been reported that a poly-L-lysin-Feridex labeling complex does not appear to affect the viability or proliferation of human MSCs, it was found that their differentiation into chondrocytes was markedly inhibited (Kostura et al., 2004), while adipogenic and osteogenic differentiation were not affected. PC-SPIO combine a low concentration of iron in the cell culture media with the high efficiency of transfection agents and thus have a broad potential for in vivo studies. However, for any intracellular label, detailed studies examining the possible biological side effects, which may vary among different cell types, are necessary.

On the other hand, particles that do not internalize do not cause any metabolic alternations and do not have any influence on cell viability or cell proliferation (Jendelova et al., 2005). Their disadvantage is that particles that do not internalize and thus stay attached to the outer cell membrane are more likely to interfere with cell surface interactions (including cell homing into tissues), may detach easily from the membrane, or may be transferred to other cells.

MR tracking may serve in experimental models to study how certain lesions target cell migration, at what speed the cells migrate, and for how long they persist in the target organ. High contrast effects on MR images are easily detected within an experimental time frame of ~1–2 h per animal, which is ideal for short and repetitive in vivo MRI. In lesioned tissue, hemorrhage products give rise to Prussian blue-positive deposits that are difficult to distinguish from iron-containing nanoparticles (Urdzikova et al., 2006). The hemorrhage degradation products may also be partially localized to macrophages because macrophages constitute the major cellular pathway for the redistribution of iron in mammals. Furthermore, hemorrhage contributes to T2 weighted hypointensity, thus interfering with the detection of labeled cells and complicating the interpretation of MR images. Therefore, it is important to determine whether cell labels remain co-localized with cell transplants, especially under pathological conditions.

With proper attention to the limitations described above, labeling cells with superparamagnetic agents would enable us to follow the migration of such cells when transplanted into humans, establish the optimal number of transplanted cells, define therapeutic windows, and monitor cell growth and possible side effects (malignancies). Currently, the described immunolabeling of specific cell types with clinically approved MicroBeads may help to elucidate the fate of implanted stem cells and evaluate the effect of cell therapy in patients with various diseases of the brain or SCI.

Abbreviations

BBB	Basso-Beattie-Bresnehan
BMCs	bone marrow cells
BrdU	bromdeoxyuridine
CNS	central nervous system
DMEM	Dulbecco's modified Eagle medium
eGFP	enhanced green fluorescent protein
EM	electron microscopy
ESCs	embryonic stem cells
G-CSF	granulocyte colony stimulating factor
HPMA	hydroxypropylmethacrylamide
LIF	leukemia inhibitory factor
Mab	monoclonal antibody
MCAO	middle cerebral artery occlusion
MR	magnetic resonance
MRI	magnetic resonance imaging
MSCs	mesenchymal stem cells
OECs	olfactory ensheathing cells
PCR	polymerase chain reaction
PC-SPIO	polycation-bound iron oxide superparamagnetic nanoparticles
SCI	spinal cord injury
SPIO	superparamagnetic iron oxide
USPIO	ultrasmall superparamagnetic iron oxide

Acknowledgment

This work was supported by grants from the Academy of Sciences of the Czech Republic AV0Z50390512, the Ministry of Education, Youth, and Sports of the Czech Republic

1M0021620803, the National Grant Agency of the Czech Republic GACR 309/06/1594, and the EC-FP6 project DiMI: LSHB-CT-2005-512146.

References

Akiyama, Y., Radtke, C., Honmou, O. and Kocsis, J.D. (2002) Remyelination of the spinal cord following intravenous delivery of bone marrow cells. Glia, 39(3): 229–236.

Anderson, S.A., Glod, J., Arbab, A.S., Noel, M., Ashari, P., Fine, H.A. and Frank, J.A. (2005) Noninvasive MR imaging of magnetically labeled stem cells to directly identify neovasculature in a glioma model. Blood, 105(1): 420–425.

Arbab, A.S., Yocum, G.T., Wilson, L.B., Parwana, A., Jordan, E.K., Kalish, H. and Frank, J.A. (2004) Comparison of transfection agents in forming complexes with ferumoxides, cell labeling efficiency, and cellular viability. Mol. Imaging, 3(1): 24–32.

Billotey, C., Wilhelm, C., Devaud, M., Bacri, J.C., Bittoun, J. and Gazeau, F. (2003) Cell internalization of anionic maghemite nanoparticles: quantitative effect on magnetic resonance imaging. Magn. Reson. Med., 49(4): 646–654.

Bjorklund, L.M., Sanchez-Pernaute, R., Chung, S., Andersson, T., Chen, I.Y., McNaught, K.S., Brownell, A.L., Jenkins, B.G., Wahlestedt, C., Kim, K.S. and Isacson, O. (2002) Embryonic stem cells develop into functional dopaminergic neurons after transplantation in a Parkinson rat model. Proc. Natl. Acad. Sci. U.S.A., 99(4): 2344–2349.

Brustle, O., Jones, K.N., Learish, R.D., Karram, K., Choudhary, K., Wiestler, O.D., Duncan, I.D. and McKay, R.D. (1999) Embryonic stem cell-derived glial precursors: a source of myelinating transplants. Science, 285(5428): 754–756.

Bulte, J.W., Ben-Hur, T., Miller, B.R., Mizrachi-Kol, R., Einstein, O., Reinhartz, E., Zywicke, H.A., Douglas, T. and Frank, J.A. (2003) MR microscopy of magnetically labeled neurospheres transplanted into the Lewis EAE rat brain. Magn. Reson. Med., 50(1): 201–205.

Bulte, J.W., Douglas, T., Witwer, B., Zhang, S.C., Strable, E., Lewis, B.K., Zywicke, H., Miller, B., van Gelderen, P., Moskowitz, B.M., Duncan, I.D. and Frank, J.A. (2001) Magnetodendrimers allow endosomal magnetic labeling and in vivo tracking of stem cells. Nat. Biotechnol., 19: 1141–1147.

Bulte, J.W., Hoekstra, Y., Kamman, R.L., Magin, R.L., Webb, A.G., Briggs, R.W., Go, K.G., Hulstaert, C.E., Miltenyi, S., The, T.H., et al. (1992) Specific MR imaging of human lymphocytes by monoclonal antibody-guided dextran-magnetite particles. Magn. Reson. Med., 25(1): 148–157.

Bulte, J.W. and Kraitchman, D.L. (2004) Iron oxide MR contrast agents for molecular and cellular imaging. NMR Biomed., 17(7): 484–499.

Bulte, J.W., Zhang, S.C., van Gelderen, P., Herynek, V., Jordan, E.K., Duncan, I.D. and Frank, J.A. (1999) Neurotransplantation of magnetically labeled oligodendrocyte progenitors: magnetic resonance tracking of cell migration and myelination. Proc. Natl. Acad. Sci. U.S.A., 96: 15256–15261.

Bulte, J.W., Zhang, S.C., van Gelderen, P., Herynek, V., Jordan, E.K., Janssen, C.H., Duncan, I.D. and Frank, J.A. (2002) Magnetically labeled glial cells as cellular MR contrast agents. Acad. Radiol., 9(Suppl 1): S148–S150.

Emsley, J.G., Mitchell, B.D., Kempermann, G. and Macklis, J.D. (2005) Adult neurogenesis and repair of the adult CNS with neural progenitors, precursors, and stem cells. Prog. Neurobiol., 75(5): 321–341.

Fairless, R. and Barnett, S.C. (2005) Olfactory ensheathing cells: their role in central nervous system repair. Int. J. Biochem. Cell. Biol., 37(4): 693–699.

Frank, J.A., Miller, B.R., Arbab, A.S., Zywicke, H.A., Jordan, E.K., Lewis, B.K., Bryant Jr., L.H. and Bulte, J.W. (2003) Clinically applicable labeling of mammalian and stem cells by combining superparamagnetic iron oxides and transfection agents. Radiology, 228(2): 480–487.

Hawrylak, N., Ghosh, P., Broadus, J., Schlueter, C., Greenough, W.T. and Lauterbur, P.C. (1993) Nuclear magnetic resonance (NMR) imaging of iron oxide-labeled neural transplants. Exp. Neurol., 121: 81–92.

Horak, D., Sykova, E., Babic, M., Jendelova, P. and Hajek, M. (2006) Superparamagnetic iron oxide nanoparticles with modified surface and their use as probes for stem cell labeling. Patent application no: PV 1006–120, Czech Republic.

Jendelova, P., Herynek, V., De Croos, J., Glogarova, K., Andersson, B., Hajek, M. and Sykova, E. (2003) Imaging the fate of implanted bone marrow stromal cells labeled with superparamagnetic nanoparticles. Magn. Reson. Med., 50: 767–776.

Jendelova, P., Herynek, V., Urdzikova, L., Glogarova, K., Kroupova, J., Bryja, V., Andersson, B., Burian, M., Hajek, M. and Sykova, E. (2004) MR tracking of transplanted bone marrow and embryonic stem cells labeled by iron oxide nanoparticles in rat brain and spinal cord. J. Neurosci. Res., 76(2): 232–243.

Jendelova, P., Herynek, V., Urdzikova, L., Glogarova, K., Rahmatova, S., Fales, I., Andersson, B., Prochazka, P., Zamecnik, J., Eckschlager, T., Kobylka, P., Hajek, M. and Sykova, E. (2005) MR tracking of human $CD34^{+}$ progenitor cells separated by means of immunomagnetic selection and transplanted into injured rat brain. Cell Transplant., 14: 173–182.

Jiang, Y., Jahagirdar, B.N., Reinhardt, R.L., Schwartz, R.E., Keene, C.D., Ortiz-Gonzalez, X.R., Reyes, M., Lenvik, T., Lund, T., Blackstad, M., Du, J., Aldrich, S., Lisberg, A., Low, W.C., Largaespada, D.A. and Verfaillie, C.M. (2002) Pluripotency of mesenchymal stem cells derived from adult marrow. Nature, 418(6893): 41–49.

Kalish, H., Arbab, A.S., Miller, B.R., Lewis, B.K., Zywicke, H.A., Bulte, J.W., Bryant Jr., L.H. and Frank, J.A. (2003) Combination of transfection agents and magnetic resonance contrast agents for cellular imaging: relationship between relaxivities, electrostatic forces, and chemical composition. Magn. Reson. Med., 50(2): 275–282.

Kostura, L., Kraitchman, D.L., Mackay, A.M., Pittenger, M.F. and Bulte, J.W. (2004) Feridex labeling of mesenchymal stem

cells inhibits chondrogenesis but not adipogenesis or osteogenesis. NMR Biomed., 17(7): 513–517.

Lee, I.H., Bulte, J.W., Schweinhardt, P., Douglas, T., Trifunovski, A., Hofstetter, C., Olson, L. and Spenger, C. (2004) In vivo magnetic resonance tracking of olfactory ensheathing glia grafted into the rat spinal cord. Exp. Neurol., 187(2): 509–516.

Lesny, P., Pradny, M., Jendelova, P., Michalek, J., Vacik, J. and Sykova, E. (2006) Macroporous hydrogels based on 2-hydroxyethyl methacrylate. Part 4: growth of rat bone marrow stromal cells in three-dimensional hydrogels with positive and negative surface charges and in polyelectrolyte complexes. J. Mater. Sci. Mater. Med., 17: 829–833.

McDonald, J.W., Liu, X.Z., Qu, Y., Liu, S., Mickey, S.K., Turetsky, D., Gottlieb, D.I. and Choi, D.W. (1999) Transplanted embryonic stem cells survive, differentiate and promote recovery in injured rat spinal cord. Nat. Med., 5(12): 1410–1412.

McKay, R.D. (2004) Stem cell biology and neurodegenerative disease. Philos. Trans. R. Soc. Lond. B. Biol. Sci., 359(1445): 851–856.

Mendonca Dias, M.H. and Lauterbur, P.C. (1986) Ferromagnetic particles as contrast agents for magnetic resonance imaging of liver and spleen. Magn. Reson. Med., 3(2): 328–330.

Newman, M.B., Davis, C.D., Borlongan, C.V., Emerich, D. and Sanberg, P.R. (2004) Transplantation of human umbilical cord blood cells in the repair of CNS diseases. Expert Opin. Biol. Ther., 4(2): 121–130.

Norman, A.B., Thomas, S.R., Pratt, R.G., Lu, S.Y. and Norgren, R.B. (1992) Magnetic resonance imaging of neural transplants in rat brain using a superparamagnetic contrast agent. Brain Res., 594: 279–283.

Orlic, D., Kajstura, J., Chimenti, S., Bodine, D.M., Leri, A. and Anversa, P. (2001a) Transplanted adult bone marrow cells repair myocardial infarcts in mice. Ann. N.Y. Acad. Sci., 938: 221–230.

Orlic, D., Kajstura, J., Chimenti, S., Jakoniuk, I., Anderson, S.M., Li, B., Pickel, J., McKay, R., Nadal-Ginard, B., Bodine, D.M., Leri, A. and Anversa, P. (2001b) Bone marrow cells regenerate infarcted myocardium. Nature, 410(6829): 701–705.

Pachernik, J., Bryja, V., Esner, M., Kubala, L., Dvorak, P. and Hampl, A. (2005) Neural differentiation of pluripotent mouse embryonal carcinoma cells by retinoic acid: inhibitory effect of serum. Physiol. Res., 54(1): 115–122.

Park, K.I., Lachyankar, M., Nissim, S. and Snyder, E.Y. (2002) Neural stem cells for CNS repair: state of the art and future directions. Adv. Exp. Med. Biol., 506(Pt B): 1291–1296.

Pittenger, M.F., Mackay, A.M., Beck, S.C., Jaiswal, R.K., Douglas, R., Mosca, J.D., Moorman, M.A., Simonetti, D.W., Craig, S. and Marshak, D.R. (1999) Multilineage potential of adult human mesenchymal stem cells. Science, 284(5411): 143–147.

Pluchino, S., Zanotti, L., Deleidi, M. and Martino, G. (2005) Neural stem cells and their use as therapeutic tool in neurological disorders. Brain Res. Brain Res. Rev., 48(2): 211–219.

Renshaw, P.F., Owen, C.S., McLaughlin, A.C., Frey, T.G. and Leigh Jr., J.S. (1986) Ferromagnetic contrast agents: a new approach. Magn. Reson. Med., 3(2): 217–225.

Roitberg, B. (2004) Transplantation for stroke. Neurol. Res., 26(3): 256–264.

Sasaki, M., Honmou, O., Akiyama, Y., Uede, T., Hashi, K. and Kocsis, J.D. (2001) Transplantation of an acutely isolated bone marrow fraction repairs demyelinated adult rat spinal cord axons. Glia, 35: 26–34.

Sykova, E. and Jendelova, P. (2005) Magnetic resonance tracking of implanted adult and embryonic stem cells in injured brain and spinal cord. Ann. N.Y. Acad. Sci., 1049: 146–160.

Sykova, E. and Jendelova, P. (2006) Magnetic resonance tracking of transplanted stem cells in rat brain and spinal cord. Neurodegener. Dis., 3: 62–67.

Sykova, E., Jendelova, P., Urdzikova, L., Lesny, P. and Hejcl, A. (2006) Bone marrow stem cells and polymer hydrogels: two strategies for spinal cord injury repair. Cell. Mol. Neurobiol., 26(7–8): 1111–1127.

Takahashi, T., Kalka, C., Masuda, H., Chen, D., Silver, M., Kearney, M., Magner, M., Isner, J.M. and Asahara, T. (1999) Ischemia- and cytokine-induced mobilization of bone marrow-derived endothelial progenitor cells for neovascularization. Nat. Med., 5(4): 434–438.

Toma, C., Pittenger, M.F., Cahill, K.S., Byrne, B.J. and Kessler, P.D. (2002) Human mesenchymal stem cells differentiate to a cardiomyocyte phenotype in the adult murine heart. Circulation, 105(1): 93–98.

Uccelli, A., Zappia, E., Benvenuto, F., Frassoni, F. and Mancardi, G. (2006) Stem cells in inflammatory demyelinating disorders: a dual role for immunosuppression and neuroprotection. Expert Opin. Biol. Ther., 6(1): 17–22.

Urdzikova, L., Jendelova, P., Glogarova, K., Burian, M., Hajek, M. and Sykova, E. (2006) Transplantation of bone marrow stem cells as well as mobilization by granulocyte-colony stimulating factor promote recovery after spinal cord injury in rat. J. Neurotrauma, 23: 1379–1391.

Zhang, Z.G., Jiang, Q., Zhang, R., Zhang, L., Wang, L., Arniego, P., Ho, K.L. and Chopp, M. (2003) Magnetic resonance imaging and neurosphere therapy of stroke in rat. Ann. Neurol., 53(2): 259–263.

Zhang, Z.Y. and Smith, B.D. (2000) High-generation polycationic dendrimers are unusually effective at disrupting anionic vesicles: membrane bending model. Bioconjug. Chem., 11(6): 805–814.

Zhao, C., Fancy, S.P., Magy, L., Urwin, J.E. and Franklin, R.J. (2005) Stem cells, progenitors and myelin repair. J. Anat., 207(3): 251–258.